Effects of Ion Irradiation on Stage II Fatigue Crack Growth and Plasticity

Melissa Weihrauch (corresponding author)

sgmweihr@liverpool.ac.uk

School of Engineering, University of Liverpool, The Quadrangle, Brownlow Hill, Liverpool L69 3GH, UK

Maulik Patel

maulik@liverpool.ac.uk

School of Engineering, University of Liverpool, The Quadrangle, Brownlow Hill, Liverpool L69 3GH, UK

Eann A. Patterson

eannp@liverpool.ac.uk

School of Engineering, University of Liverpool, The Quadrangle, Brownlow Hill, Liverpool L69 3GH, UK

Key Words: Fatigue Crack Growth, Thermoelastic Stress Analysis, Ion Irradiation, Plastic Zone, Secondary Cracking, Stage II Fatigue

No potential conflict of interest is declared by the authors. Melissa Weihrauch was supported by a PhD studentship funded jointly by Rolls-Royce plc and by the EPSRC Centre for Doctoral Training entitled GREEN: Growing skills for Reliable Economic Energy from Nuclear. All information and intellectual property generated by this research work is the property of Rolls-Royce Plc. Experimental data has been provided in the supplementary files.

Abstract

Fatigue crack growth characteristics of ion irradiated compact tension specimens were evaluated in the Paris law region. Fatigue crack growth was monitored under tension-tension loading and the thermoelastic response was measured. Two stages of crack propagation were identified. In the first 300,000 cycles, crack growth rates of irradiated and unirradiated specimens were comparable and plastic zone area was found to be independent of crack length. Beyond 300,000 cycles, irradiated specimens showed a greater crack growth rate; additionally, the plastic zone area increased with crack length. The increase in crack growth rate was attributed to irradiation hardening. The plastic zone area was found to be dependent on the crack path, especially in the initial stages of crack propagation. Local peaks in the value of the area of the plastic zone were found to be associated with greater crack tortuosity and secondary cracks. As a result, decreases in plastic zone area were associated with greater crack growth rates.

Introduction

Austenitic stainless steels are widely used in the nuclear industry as structural components. Fatigue damage is an active degradation mechanism in these materials, especially as reactor service lifetimes are being extended. Therefore, knowledge of how fatigue life times are affected by irradiation damage and the nature of fatigue crack propagation under these conditions is essential.

Radiation damage is a degradation mechanism in nuclear reactor environments. Changes in the mechanical properties of structural materials induced by neutron irradiation can be a limiting factor in reactor life times[1]. Internal components in the core, usually made of austenitic stainless steels, can experience tens of displacement per atom (dpa) over a reactor's lifetime. Neutrons produce interstitial-vacancy pairs in materials within picoseconds[2]. These interstitial-vacancy pairs either recombine or migrate away from one other to produce larger defects (e.g. dislocations). The exact nature of the defects depend on multiple factors, including dose rate, temperature, and total accumulated dose.

At temperatures below 40% of the melting temperature of a material, defect clusters can impede dislocation motion resulting in hardening[1]. In austenitic steels, increases in hardness of up to 92% have been reported from heavy ion irradiation at room temperature [3,4]. In stainless steels, below temperatures of 300˚C, black dot damage outweighs Frank dislocation loops[5]. While at greater temperatures much larger Frank dislocation loops are observed. Black dots are small defect clusters of either vacancies or interstitials. Frank dislocation loops can grow from black dots as more interstitials cluster together. At higher temperatures, radiation can cause swelling and segregation of alloying elements, making them vulnerable to corrosion. Depletion of chromium and iron and enrichment of nickel have been observed at grain boundaries of neutron irradiated 304 stainless steels at 288˚C [6].

Experiments with neutron irradiation are highly time and resource intensive due to the limited availability of research reactors, relatively low neutron fluxes, and activation of samples. This makes irradiations to relevant damage levels time consuming and costly. Ion irradiation has become a commonly used alternative to replicate neutron damage. However, ion irradiations can result in shallow implantation depths in relation to the specimen thickness and can produce a non-uniform damage profile. Nevertheless ion irradiation has been established as a useful technique to emulate neutron damage, with comparable results between ion and neutron irradiations having been obtained[7–9].

The increase in hardness, fracture toughness, and yield strength caused by irradiation also has an impact on fatigue life. It is usually assumed that in austenitic steels high cycle fatigue life is increased by neutron irradiation due to increased yield strength, while low cycle fatigue life is reduced due to increased hardness[2]. Studies on ferritic/martensitic steel have shown various effects on fatigue life. For example, neutron irradiation at 115 ˚C and He ion implantation at 470˚C reduced low cycle fatigue life at high strains ($\Delta\varepsilon$>1 %), while no change in fatigue life was reported when irradiations occurred at lower strains[10]. A different study on reduced activation ferritic/martensitic steel irradiated with neutrons at 330 ˚C found increased low cycle fatigue life times at low strains ($\Delta\varepsilon$<0.9 %), and reduced fatigue life times at high strains ($\Delta\varepsilon$>0.9 %) [11]. For 316LN stainless steel, no difference in low cycle fatigue life was observed after high temperature irradiation between 450 and 750 ˚C and fatigue testing at 550 ˚C [12]. Specimens of 304 stainless steel irradiated with protons at 350 ˚C showed a slightly increased fatigue life[13]. Fenici and Suolang found that 316 stainless steel irradiated in situ with protons had an increased time to crack to initiation[14]. In situ low cycle fatigue tests of 316L steel during neutron irradiation showed no significant changes compared to un-irradiated specimens[15]. A summary of the discussed results are shown in table I.

Table I: A summary of findings from literature on the effect of irradiation on fatigue crack growth in steels

Material	Irradiation Type	Irradiation Temperature (˚C)	Fatigue Test Conditions	Effect on Fatigue Life	Ref
Ferritic/Martensitic Steel	Neutrons	115	Low cycle strain-controlled fatigue $\Delta\varepsilon>1\%$ at room temperature	Reduction in number of cycles to failure	10
Ferritic/Martensitic Steel	50 MeV He ions	470	Low cycle strain-controlled fatigue $\Delta\varepsilon>1\%$ at room temperature	Reduction in number of cycles to failure	10
Reduced activation Ferritic/Martensitic Steel	Neutrons	330	Low cycle strain-controlled fatigue $\Delta\varepsilon<0.9$ % at room temperature	Increase in number of cycles to failure	11
Reduced activation Ferritic/Martensitic Steel	Neutrons	330	Low cycle strain-controlled fatigue $\Delta\varepsilon>0.9$ % at room temperature	Reduction in number of cycles to failure	11
316 CL Stainless Steel	Neutrons	550	Low cycle strain-controlled fatigue at 550C $\Delta\varepsilon>1$ %	No change	12
304 Stainless Steel	1.6 MeV Protons	350	High cycle load-controlled fatigue at room temperature	Increase in number of cycles to failure	13
316 Stainless Steel	20 MeV Protons	130-300	Low cycle load-controlled fatigue during irradiation	Increased time to crack initiation	14
316L Stainless Steel	Neutrons	250	Low cycle load-controlled fatigue during irradiation	No change	15

From table I, it is apparent that no clear consensus exists on the impact of irradiation on fatigue life. Different results suggest either a reduction, an increase or no change in cycles to failure. Due to experimental constrains, many studies have been focused on low cycle fatigue. In many of the discussed studies, failure occurred within 100,000 cycles covering all stages of growth from crack initiation to failure. Past results suggest that irradiation delays crack initiation and stage I crack propagation. These stages take up the majority of cycles in a fatigue test, and therefore not much data on the later stages of crack growth is available. This study will use precracked specimens to focus on stage II crack propagation. The effects of ion irradiation on stage II fatigue crack growth in austenitic 316LN steel will be evaluated through the continuous monitoring of the crack tip location and plastic zone size during loading.

Fatigue crack growth can be divided into three stages: initiation and short crack formation, long crack propagation, and rupture. Initiation and short crack propagation, or stage I crack growth, comprises the majority of a component's fatigue life. Stage I propagation occurs when the plastic zone size is smaller than a few grains. As a result, the behaviour of short cracks is highly dependent on microstructural factors, including crystal structure, grain size, plastic zone size, and inclusions [16]. Short crack propagation occurs via planar slip. Preferential slip planes vary depending on a material's crystal lattice, for instance, the preferred slip plane for fcc materials is the {111} plane in the <110> direction[17]. Propagation by slip leads to a highly tortuous or zig-zag crack path. Additionally, grain boundaries can serve to retard crack growth and introduce further tortuosity.

For long crack propagation, or stage II crack propagation, the crack growth rate can be described by the Paris-Erdogan law in equation 1[18]:

$$\frac{da}{dN} = C(\Delta K)^m [1]$$

where a is the crack length, N are the elapsed fatigue cycles, ΔK is the change in stress intensity factor and C and m are constants. In the Paris region (stage II crack propagation), the crack propagates normal to the load axis (assuming mode I loading) via slip of two planes at roughly 45° angles to the main crack[19,20]. During stage II crack propagation, the plastic zone encompasses many grains and crack growth is assumed to be largely insensitive to microstructural features[21]. However, some microstructural dependence has been reported in long cracks. In multiphase eutectic aluminium alloys, increased plastic zone size has been found to lead to greater tortuosity[22]. In multiphase steel, Birkbeck *et al.* found that in the initial phase of stage II crack propagation, where the plastic zone area and stress intensity factors were small, the crack path was dependant on the microstructure. Hence, it was suggested that the Paris region should be divided into a microstructurally sensitive and insensitive one, stage IIa and stage IIb[23]. Notably, the constants C and m remained constant through the Paris region[23]. This suggests that cracks propagating near threshold stress intensity factors at low growth rates have a higher sensitivity to microstructure.

The motivation of this study was to gain insight into crack growth behaviour in irradiated 316LN stainless steel in which a crack had already developed. Thus, this study aims to improve understanding of how irradiation effects stage II fatigue crack propagation. To do so plastic zone size and crack growth rates have been measured and correlated to microstructural changes. Thermoelastic stress analysis (TSA) was used to monitor crack propagation and to study the instantaneous material response during fatigue.

Methods

Precracking

Compact tension (CT) specimens with dimensions of 25 x 24 x 0.8 mm were manufactured from nuclear grade 316LN austenitic steel. A technical drawing of the CT specimens has been supplied in the supplementary data. Rickerby and Fenici have shown the validity of the use thin CT specimens to obtain meaningful crack growth information in 316 type steel[24]. The specimens were polished using a Buehler automated polisher (AutoMet™ 250 Grinder-Polisher, Buehler, Lake Bluff, IL) with SiC abrasive paper up to a grit size of P800 on both surfaces. A single surface was polished to a mirror finish with a 1-micron diamond paste and colloidal silica.

As per ASTM E647, a one millimetre long pre-crack was initiated in the specimen to mitigate effects from the machined notch and its plastic zone on crack growth[25]. Specimens were loaded with an Electropuls E3000 (Instron, Norwood, MA, USA). To generate the pre-crack in a viable timeframe a reducing load procedure was implemented at a test frequency of 80 Hz [13]. The initial load was 600±200N, and every 30,000 cycles the mean load and amplitude were reduced by 30 N and 10 N respectively, keeping R-ratio at a constant of 0.5. When a load of 450±150 N was reached, the load was maintained until a crack of 1 mm had grown.

The thermoelastic response during pre-cracking was monitored with a cooled IR camera (SC750 InSb, FLIR). Samples were prepared with black paint (Graphit 33, Kontakt Chemie, Germany) to produce uniform surface emissivity and a sample surface that approximated that of a black body. Uncalibrated TSA images were generated in real-time through the DeltaTherm software (Stress Photonics Inc. Maddison, WI, USA). The crack length was estimated from the phase images of TSA data. To identify the crack tip, the point at which the phase signal moved from negative to positive was found with the procedure described by Díaz *et al*.[26]. It should be noted that a different method was used to identify the crack tip during the main fatigue experiment, as TSA data was processed in a somewhat different manner which will be described in subsequent sections.

Ion Irradiations

Precracked CT specimens were irradiated with 30 MeV Ni^{6+} ions at the Dalton Cumbrian Facility using a 5 MV Tandem accelerator. A 10 x 10 mm area on the mirror finished surface of the specimen was irradiated, the irradiated region has been marked in the dashed lines of figure S1 in the supplementary files. Two specimens were irradiated to a damage level of 1 dpa (fluence of 1.1×10^{15} Ni cm^{-2}) and a single specimen was irradiated to 3 dpa (3.4×10^{15} Ni cm^{-2}) at an ion flux of 10^{11} Ni $cm^{-2}s^{-1}$. Additionally, two sister samples for nanoindentation tests with dimensions of (5 x 5 x 1 mm) were irradiated to 1 and 3 dpa under the same irradiation conditions. The expected irradiation depth of peak damage was 4.2 µm as calculated using the SRIM software[27]. As per the recommendations by Stoller *et al.* displacement energy and binding energy were set to 40 eV and 0 eV respectively [28]. Statistical uncertainty from the computations were minimised by following the guidance of Zinkle *et al.* and setting the number of incident ions to 20,000 [29]. The damage profile and ion implantation profile are shown in figure 1. The low levels of scatter in the figure suggest low levels of computational uncertainty.

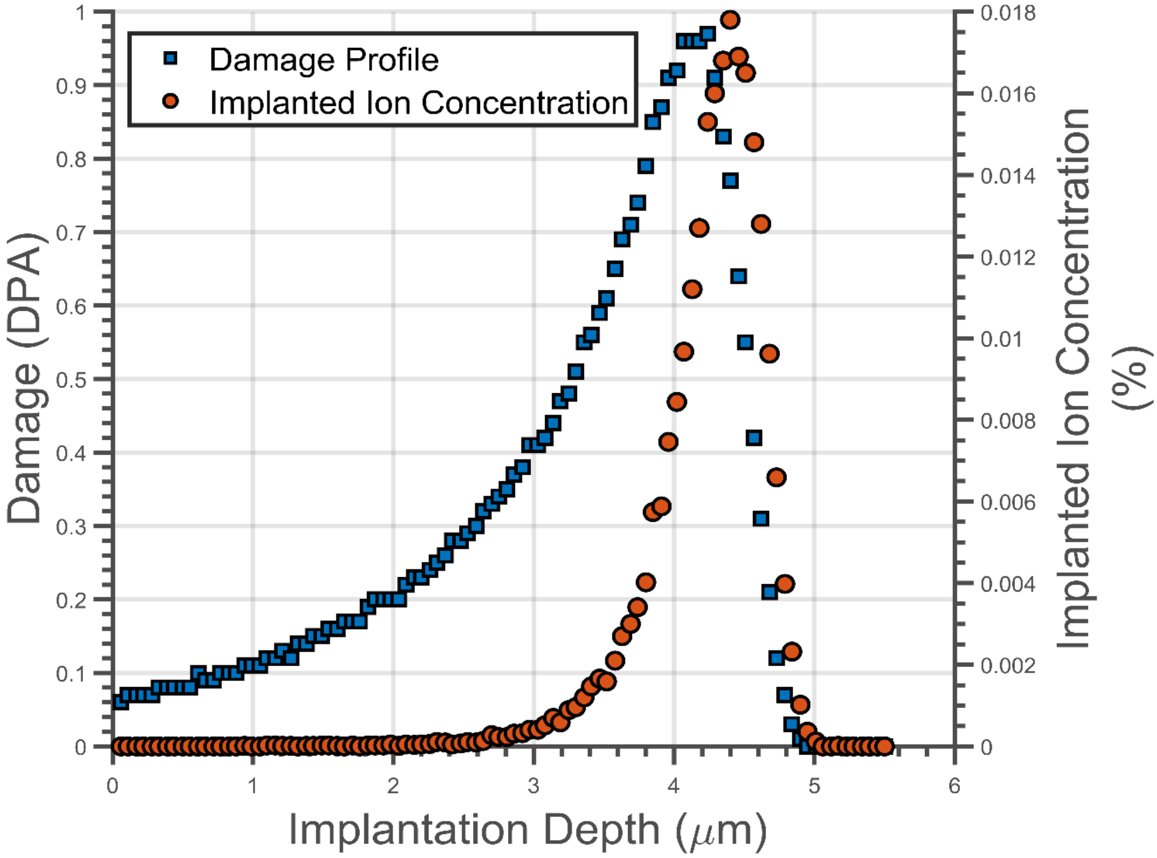

Figure 1: Expected damage profile of a specimen irradiated to 1 dpa with Ni ions corresponding to a fluence of 1.1 x 10^{15} ion cm^{-3} (squares on left axis) and the resulting implanted Ni concentration (circles on the right axis).

Crack monitoring

The pre-cracked CT specimens were sinusoidally loaded at 450±150 N at 20 Hz. A fifteen second sequence of infrared images was collected in two-minute intervals with ResearchIR software (FLIR, Wilsonville, OR, USA). In-phase and out-of-phase TSA data were produced from IR images via a lock-in amplification procedure using a purpose-written MATLAB script. Further information on producing TSA data has been provided by Greene et al [30]. The in-phase TSA images showed elastic material deformation, while the out-of-phase images represented irreversible processes. As plastic deformation is an irreversible process caused by dislocation motion, information on the plastic zone ahead of the crack tip could be obtained from the out-of-phase TSA images [31].

The plastic zone area was found from out-of-phase TSA images (Y-image) using a similar methodology to that described by Patki and Patterson [32]. The Y-image was separated into clusters by K-means segmentation. Clusters comprising the plastic zone were then identified to produce a binary image of the plastic zone. The crack tip location was defined as the coordinates of the edge of the plastic zone closest to the notch. It should be noted that crack length has been defined as the horizontal distance from the centre of the grip holes to the crack tip.

Nanoindentation

Nanohardness of unirradiated, 1 dpa, and 3 dpa irradiated sister specimens were measured with a Nano Indenter G200 (Agilent Technologies, Santa Clara, CA, USA). All indents were made with a Berkovich indenter at a displacement rate of 10 nm/s and a hold time of 10 s with 12 repeats per indent. Outliers were automatically removed by the software during nanohardness calculations. For the 3 dpa irradiated specimen, hardness was recorded at five indent depths between 160 and 800 nm. The not irradiated and 1 dpa specimen was used to obtain a more accurate picture of how hardness varied with indent depth, therefore hardness was measured at 13 indent depths between 100 and 2000 nm.

Data was fit to the Nix- Gao model to estimate bulk equivalent hardness, H_0, given in equation 2[33]. This model considered the number of geometrically necessary dislocations during the nanoindentation process.

$$\mathrm{H} = H_0 \times \sqrt{1 + \frac{h^*}{h}} \; [2]$$

Where *H* is the hardness at a given indent depth, *h* is indent depth, H_0 is the hardness at an infinite indentation depth, and h^* is a characteristic length that depends on indenter shape and other material properties. It should be noted that h^* can also be dependent on external factors such as surface roughness and friction between the indenter tip and the specimen, therefore its value can be sensitive to experimental error.

Results

Fatigue crack growth data for unirradiated, 1 dpa, and 3 dpa specimens is shown in figure 2. The fatigue tests data consisting of elapsed cycles and crack length has been provided in the supplementary data. Of the four tested unirradiated specimens, a single specimen exhibited an atypically high crack growth rate and failed within 2.7 x 10^5 cycles. As all other specimens exhibited good agreement in crack growth behaviour and failed in the order of 7 x 10^5 cycles, the specimen was classified as an outlier and excluded from data analysis.

Figure 2 shows that irradiated specimens showed a larger fatigue crack growth rate and lower cycles to failure than unirradiated ones. No clear difference in crack growth rate could be seen between the 1 and 3 dpa specimens. The scatter between repeats of each dataset was 7.1% for unirradiated specimens and 8.3% for the irradiated specimens. The initial crack growth rate was relatively constant for all tested specimens. After around 300,000 cycles, at a crack length 5.6 mm, crack growth rate was greater in the irradiated specimens.

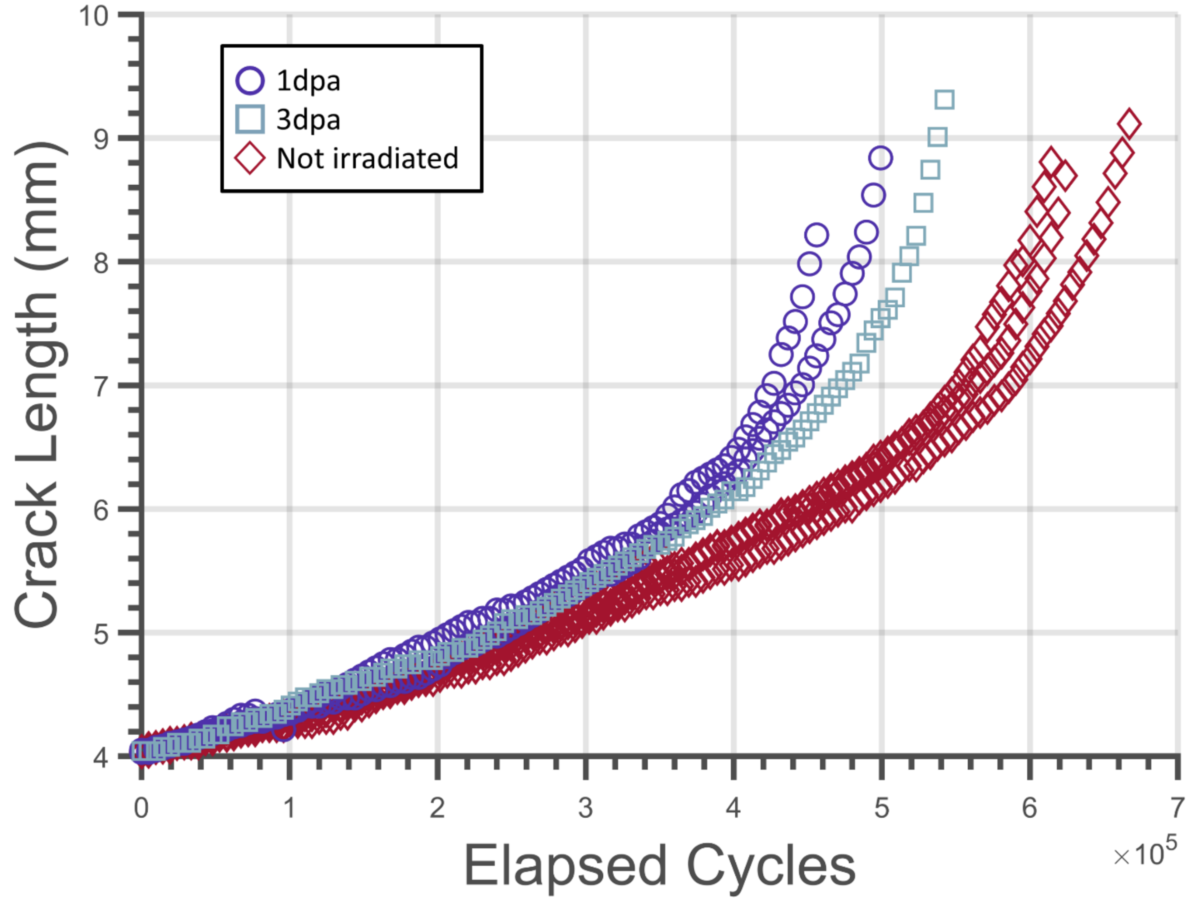

Figure 2: Crack length with cycles of non-irradiated (diamonds), 1 dpa irradiated (circles), and 3 dpa irradiated specimens (squares)

Nanoindentation results, displayed in figure 3, showed an increase in hardness by a third following irradiation. The nanoindentation data of the non-irradiated, 1 dpa and, 3 dpa specimens have been provided in the supplementary data files. The error bars in figure 3 indicate a low error in the data of the pristine specimen. The uncertainties of irradiated specimens, especially at shallow indent depths, was larger due to surface imperfections developed during the handling of specimens for irradiations. Furthermore, figure 3 shows that hardness values of the 1 and 3 dpa specimens were comparable. By fitting data to the Nix-Gao model (equation 2), the bulk hardness of the specimens was obtained. Table II shows all fitted parameters as well as its R^2 value to quantify the goodness of fit. The R^2 value of irradiated specimens was less than that of the pristine one as the irradiation damage level, and therefore hardness, were not constant with depth. The bulk hardness of the non-irradiated specimens was 1.84 GPa, while it was 2.99 GPa and 3.02 GPa for the 1 and 3 dpa specimens respectively. These values are comparable to those found in the literature[3,4,34]. For instance, Yabuuchi *et al.* measured the hardness of unirradiated 316L stainless steel to be 1.5 GPa, with the hardness increasing to 5.3 GPa after irradiation with protons to 8 dpa[34]. Nanoindentation results in this study additionally suggest that the magnitude of irradiation hardening with damage level reached a plateau, an observation that has also been made in literature [3,4].

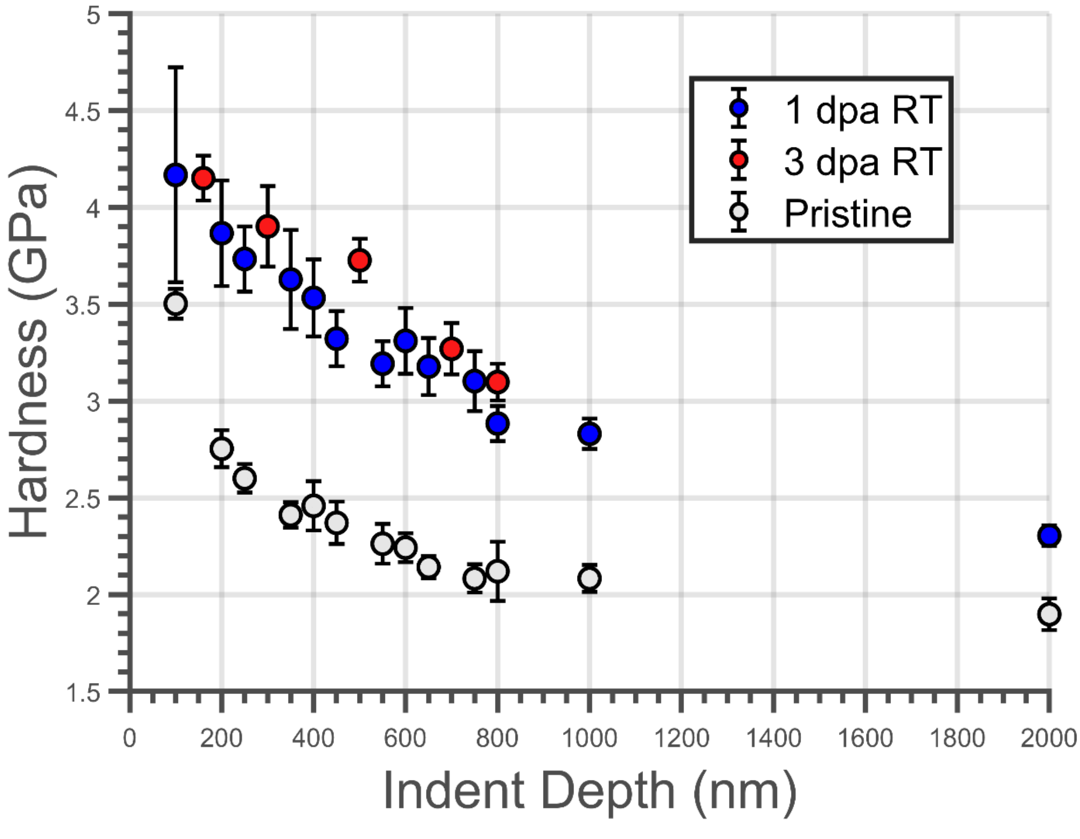

Figure 3: Nanoindentation results of not irradiated (pristine), 1 dpa, and 3 dpa Ni irradiated specimens.

Table II: Fitted Nix-Gao parameters obtained from nanoindentation data and R^2 value of fit

Specimen	Bulk Hardness, H_0 (GPa)	h* (nm)	R^2
Not Irradiated	1.84	263.2	0.99
1 dpa RT	2.99	115.6	0.83
3 dpa RT	3.02	159.2	0.8

The evolution of the plastic zone area during the fatigue tests is shown in figure 4. No clear differences between irradiated and unirradiated specimens could be observed. The data from all specimens exhibited a large level of scatter and variable plastic zone sizes. The plastic zone area appeared to behave independently of the crack length up to a crack length of 5.6 mm. At larger crack lengths. the plastic zone size increased more steadily and showed less scatter. Notably, 5.6 mm also corresponded to the crack length after which variations in crack growth rate occurred between non-irradiated and irradiated specimens.

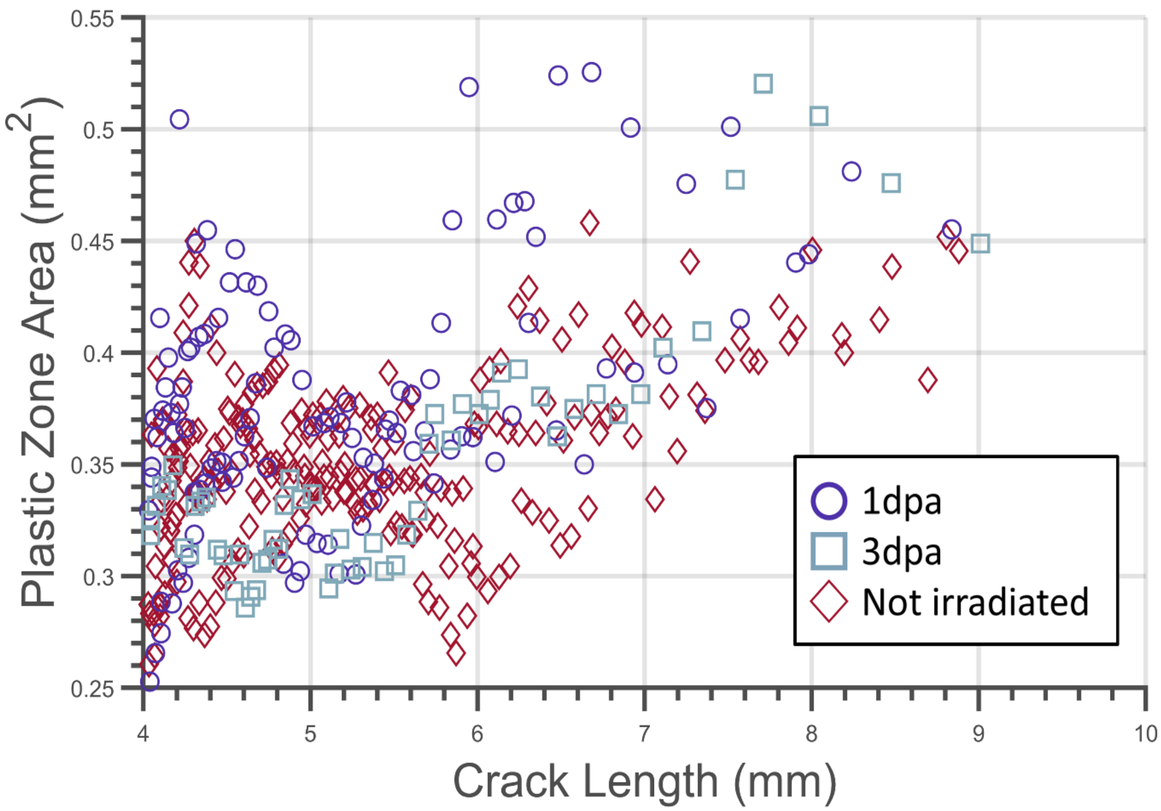

Figure 4: Plastic zone area variation with crack length of un-irradiated (diamonds), 1 dpa irradiated (circles) and 3 dpa irradiated (squares) CT specimens

Microscopy was used to understand the causes of the large scatter and the peaks in plastic zone area with crack length that is seen in figure 4. A specimen that was irradiated to 1 dpa was analysed under an optical microscope with brightfield illumination in reflective mode, see Figure 5, and in a scanning electron microscope (SEM), see figure 6, after fatigue failure. Optical microscopy was used to observe the crack path of the specimen, while the SEM was used to investigate the fatigue fracture surface.

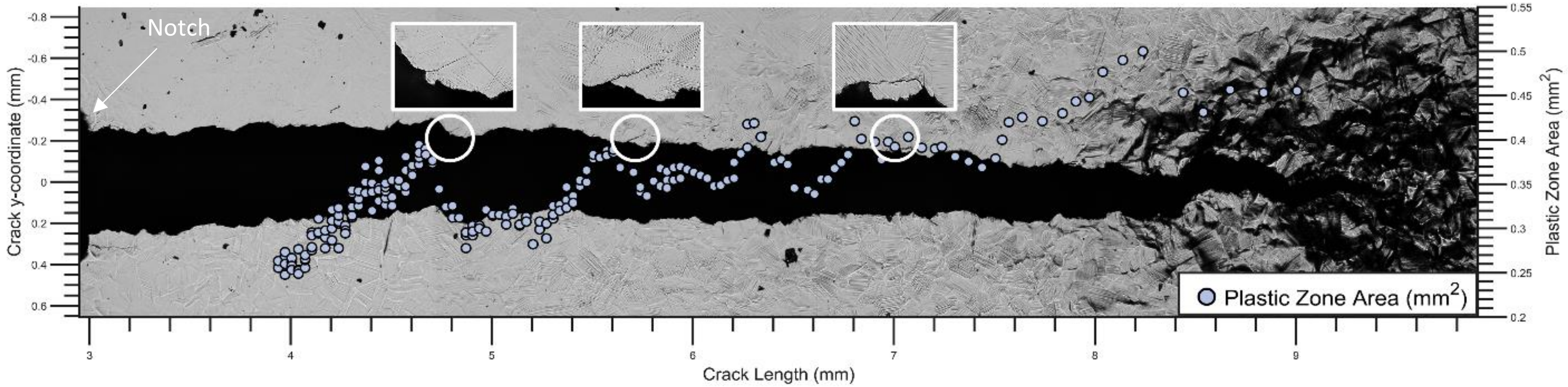

Figure 5: Optical microscopy image of fatigue crack of a CT specimen irradiated to 1 dpa with plastic zone area overlayed.

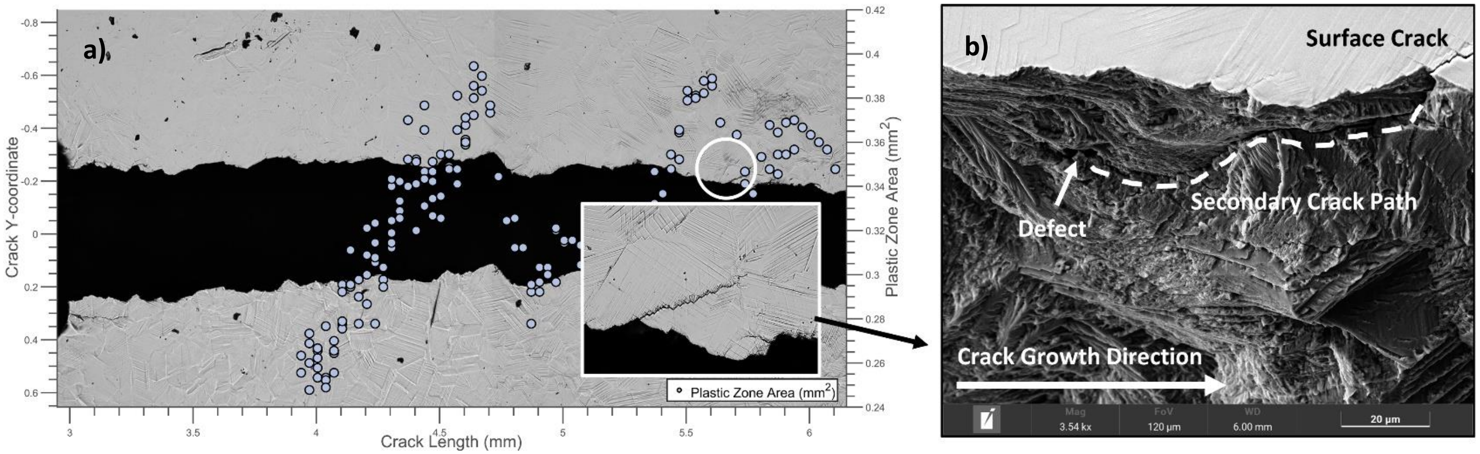

Figure 6: a) Optical microscopy image of a CT specimen irradiated to 1 dpa and the plastic zone size at the corresponding crack tip position. The circled area marks the region viewed with an SEM in b).

The plastic zone area overlaid on an optical microscopy image can be seen in figure 5. The optical microscopy image shows high levels of plasticity around the crack indicated by surface texture with slip bands and some twinning. Figure 5 shows that peaks in the plastic zone area are associated with secondary cracks. Three examples of this at crack lengths between 4.6 and 7.2 mm have been highlighted. Additionally, high levels of crack tortuosity can be seen around the peaks in plastic zone area (e.g., at 4.6 mm and 6.2 mm).

The fatigue fracture surfaces of the same specimen were examined under a SEM. Areas containing secondary cracks were of particular interest. The secondary crack circled in figure 6a has been examined closer under the SEM image seen in figure 6b. The SEM image revealed that the secondary crack originated from a defect, possibly a void, located around 20 μm below the surface. The crack propagated internally for 300 μm before becoming visible as a secondary surface crack. This secondary crack path followed slip bands that formed through the plastic deformation ahead of the main crack tip.

The expected impact of a larger plastic zone size, and hence increased crack tortuosity and secondary cracks was a reduction in crack growth rate. Figure 7 shows crack growth rate (blue squares) and plastic zone area (brown circles) on separate axes. Sections in which plastic zone area decreased have been highlighted. The figure shows that a drop in plastic zone area coincided with an increase in crack growth rate. This indicates that areas of less tortuosity had a higher crack propagation rate. However, it should be noted that the low sample size in this investigation limited the extent of possible statistical analysis.

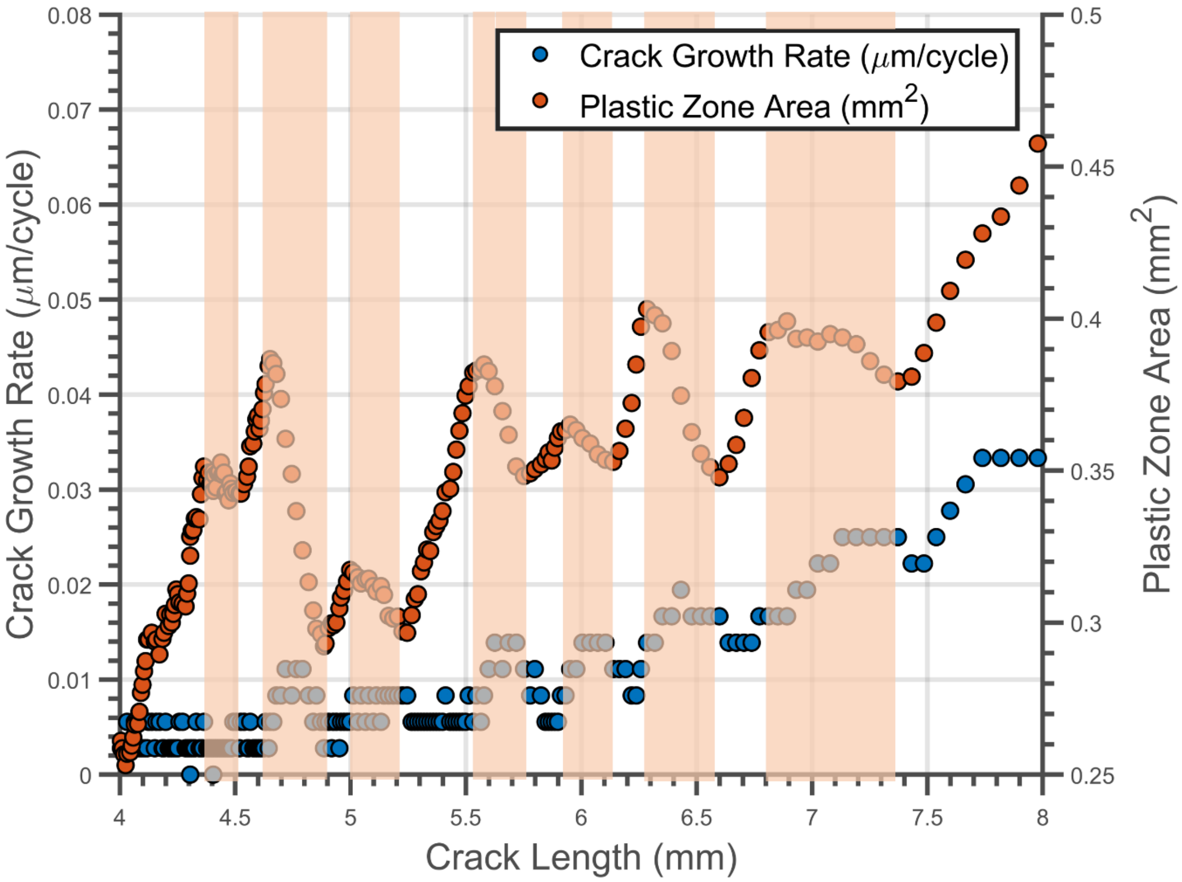

Figure 7: Crack growth rate and plastic zone area at different crack length of a CT specimen irradiated to 1 dpa

Discussion

Fatigue tests showed that irradiation negatively impacted the fatigue life of pre-cracked 316LN CT specimens irradiated with Ni ions at room temperature. Despite the small sample size, the crack growth rates of the irradiated specimens were consistently greater than in the unirradiated group. Two phases of fatigue crack growth were identified from experimental results. In the initial 300,000 cycles (corresponding to a nominal crack length of 5.6 mm), crack growth rate was unaltered by irradiation with Ni ions at room temperature. During the same stage, size of the plastic zone area appeared to be independent of the crack length.

In the second phase, crack growth rate of irradiated specimens increased compared to the unirradiated ones. Additionally, the plastic zone area became dependent on crack length. The coincidence of both effects indicates a change in crack propagation mechanism in the studied 316 LN CT specimens. It has previously been suggested that crack growth in the Paris region can be subdivided into a microstructurally-dependant phase, stage IIa, and an independent phase, stage IIb[23]. Irradiation damage from the current study was not expected to cause any significant changes in the high-level microstructure. Due to the low irradiation temperature, radiation induced segregation and by extension precipitate formation, phase changes, and void nucleation were unlikely [2,3536]. No meaningful differences in the X-ray diffraction (XRD) spectra of irradiated and unirradiated specimens were found, indicating no texture or phase changes. Previously grazing incidence XRD (GIXRD) analysis of Xe irradiated austenitic steel revealed no peak broadening or phase changes at damage levels under 7 dpa[37]. However, a decrease in peak angle has been found in XRD[38] and GIXRD[39] data of ion irradiated 316 steel. The change in peak location was attributed to increased lattice distortion from dislocation loops produced during irradiation[38,39].

In this investigation at the microstructurally-independent stage IIb, the crack could exhibit greater sensitivity to changes in mechanical properties caused by irradiation. In austenitic steels, increases in hardness of up to 92% have been reported from heavy ion irradiation at room temperature [3,4]. In this study a hardness increase of 63% was measured as a result of 30 MeV Ni ion irradiation at room temperature. Irradiation hardening is attributed to the increased number of dislocations, such as Frank loops, and black dots[2]. Room temperature ion irradiation studies have reported dislocation loop sizes in the range of 5 to 7 nm and loop densities between 2.7 x10^{22} m^{-3} and 4.3 x10^{22} m^{-3}[38–40]. The hardening attributed to these dislocations could have influenced stage IIb crack propagation, and led to a faster crack growth rate in the irradiated specimens of this study.

In previous investigations, the effect of irradiation hardening has been found to saturate at around 1 dpa[3,4]. A similar effect was observed in this study as no significant difference in nanohardness was seen between the 1 dpa and 3 dpa irradiated specimens, which helps explain the similarity in fatigue crack growth rates for all irradiated specimens regardless of damage level.

Past studies have reported no change or only a slight increase in fatigue life caused by irradiation[2,10–13,15]. While this study found an overall decrease in fatigue life, caused by irradiation, stage II crack growth was examined here, meaning that crack initiation and short crack propagation were not considered. Additionally, large variations in irradiation procedures exist between this study and others, including ion energy and type, irradiation temperature, and flux leading to the large variation in experimental results. For instance, the degree of radiation hardening at high temperatures is less pronounced, which would in turn effect fatigue life[4,41].

To understand how fluctuations in plastic zone area were correlated to the crack path, optical micrographs and SEM images of a cracked irradiated specimen were studied. Results showed that increases in plastic zone area correlated with crack tortuosity and secondary cracks in the investigated 316LN CT specimens. Secondary cracks propagated along the slip bands or were formed by the accumulation of slip bands.

The plastic zone area also impacted crack propagation rates as reductions in plastic zone area correlated with increases in crack growth rate in the tested CT specimens. Conceptually this can be explained by large plastic zone areas being associated with crack deflection and secondary crack formation. Hence, energy was expended in the form of dislocation motion, crack deflection, and the forming of secondary cracks instead of advancing the primary crack.

Conclusion

In this investigation stage II fatigue crack growth in compact tension specimens irradiated with 30 MeV Ni^{6+} ions were studied. Thermoelastic stress analysis was used to monitor crack growth and calculate plastic zone area, and the crack path and fracture surface were observed after fatigue tests. Additionally, irradiation hardening was measured through nanoindentation. An increase in crack growth rate was found in irradiated specimens which was attributed to irradiation hardening despite the shallow implantation depth. Results from the 316LN stainless steel compact tension specimens indicate that two phases of stage II crack growth exist. In the first phase, crack growth rate in the specimens irradiated with 30 MeV Ni ions at room temperature and unirradiated specimens were equal. At this stage plastic zone area appeared unaffected by crack length. At later stages, when the plastic zone area of the tested specimens began increasing with crack length, the crack propagated faster in irradiated specimens. This was attributed to an increase in hardness of the irradiated specimens. Additionally, increases in plastic zone area were found to be associated with high levels of crack tortuosity and secondary cracks. Hence, when plastic zone area was reduced in the investigated specimens, crack growth rate increased.

Acknowledgements

We acknowledge the support of The University of Manchester's Dalton Cumbrian Facility (DCF), a partner in the National Nuclear User Facility, the EPSRC UK National Ion Beam Centre and the Henry Royce Institute. We recognise Carl Andrews and Samir de Moraes Shubeita for their assistance during Ni ion irradiations.

The authors would like to acknowledge the support of the Materials Innovation Factory at the University of Liverpool, created as part of the UK Research Partnership Investment Fund (UKRPIF) initiative, managed by UKRI Research England. We would also like to express our thanks to Sir Henry Royce Institute, the UK's National Institute for advanced materials research and innovation, which funded the some of the equipment used to undertake this research. Specifically, we would like to thank Owen Gallagher for assistance with scanning electron microscopy work.

Additionally, the authors acknowledge the work of Fabio Bohns and Riaz Akhtar of the University of Liverpool in conducting nanoindentation experiments.

The authors would like to thank Nick Riddle and Jonathan Mann of Rolls-Royce plc for many fruitful discussions about the design of the experiments and the interpretation of the results. MW was supported by a PhD studentship funded jointly by Rolls-Royce plc and by the EPSRC Centre for Doctoral Training entitled GREEN: Growing skills for Reliable Economic Energy from Nuclear. Export Control Rating: Not Listed 28/07/23.

References

1. Zinkle, S. J. & Busby, J. T. Structural materials for fission & fusion energy. *Mater. Today* **12**, 12–19 (2009).

2. Was, G. S. *Fundamentals of Radiation Damage Materials Science, 2nd edition*. *Fundamentals of Radiation Materials Science* (2017).

3. Xu, C., Zhang, L., Qian, W., Mei, J. & Liu, X. The Studies of Irradiation Hardening of Stainless Steel Reactor Internals under Proton and Xenon Irradiation. *Nucl. Eng. Technol.* **48**, 758–764 (2016).

4. Karpov, S. A. *et al.* Hardening of SS316 stainless steel caused by the irradiation with argon ions. *Mater. Sci.* **52**, 377–384 (2016).

5. Edwards, D. J., Simonen, E. P. & Bruemmer, S. M. Evolution of fine-scale defects in stainless steels neutron-irradiated at 275 °C. *J. Nucl. Mater.* **317**, 13–31 (2003).

6. Kenik, E. A. & Busby, J. T. Radiation-induced degradation of stainless steel light water reactor internals. *Mater. Sci. Eng. R Reports* **73**, 67–83 (2012).

7. Was, G. S. *et al.* Emulation of reactor irradiation damage using ion beams. *Scr. Mater.* **88**, 33–36 (2014).

8. Was, G. S. Challenges to the use of ion irradiation for emulating reactor irradiation. *J. Mater. Res.* **30**, 1158–1182 (2015).

9. Jiao, Z., Michalicka, J. & Was, G. S. Self-ion emulation of high dose neutron irradiated microstructure in stainless steels. *J. Nucl. Mater.* **501**, 312–318 (2018).

10. Nogami, S., Hasegawa, A. & Yamazaki, M. Fatigue properties of ferritic/martensitic steel after neutron irradiation and helium implantation. *Nucl. Mater. Energy* **24**, 100764 (2020).

11. Gaganidze, E. *et al.* Low cycle fatigue properties of reduced activation ferritic/martensitic steels after high-dose neutron irradiation. *Nucl. Fusion* **51**, (2011).

12. Aktaa, J., Horsten, M. G. & Schmitt, R. Effects of hold time and neutron irradiation on the low-cycle fatigue behaviour of type 316-CL and their consideration in a damage

model. *Nucl. Eng. Des.* **213**, 111–117 (2002).

13. Spencer, R. P. & Patterson, E. A. Observations of fatigue crack behaviour in proton-irradiated 304 stainless steel. *Fatigue Fract. Eng. Mater. Struct.* **42**, 2120–2132 (2019).

14. Fenici, P. & Suolang, S. Fatigue crack growth in 316 type stainless steel at temperatures and displacement damage rates representative for the first wall loading. *J. Nucl. Mater.* **191**–**194**, 1408–1412 (1992).

15. Vandermeulen, W., Hendrix, W., Massaut, V. & Van de Velde, J. The effect of neutron irradiation on the fatigue behaviour of AISI 316L - Results of first in-pile tests. *J. Nucl. Mater.* **183**, 57–61 (1991).

16. Lankford, J. the Influence of Microstructure on the Growth of Small Fatigue Cracks. *Fatigue Fract. Eng. Mater. Struct.* **8**, 161–175 (1985).

17. Wilson, D., Wan, W. & Dunne, F. P. E. Microstructurally-sensitive fatigue crack growth in HCP, BCC and FCC polycrystals. *J. Mech. Phys. Solids* **126**, 204–225 (2019).

18. Paris, P. & Erdogan, F. A critical analysis of crack propagation laws. *J. Fluids Eng. Trans. ASME* **85**, 528–533 (1963).

19. Grinberg, N. M. Stage II fatigue crack growth. *Int. J. Fatigue* **6**, 229–242 (1984).

20. Ritchie, R. O. Mechanism of Fatigue-Crack Propagation in Ductile and Brittle Materials. *Int. J. Fract.* **100**, 55–83 (1998).

21. Suresh, S. *Fatigue of Materials*. (Cambridge University Press, 1998). doi:10.1017/CBO9780511806575.

22. Lados, D. A., Apelian, D. & Major, J. F. Fatigue crack growth mechanisms at the microstructure scale in Al-Si-Mg cast alloys: Mechanisms in Regions II and III. *Metall. Mater. Trans. A Phys. Metall. Mater. Sci.* **37**, 2405–2418 (2006).

23. Birkbeck, G., Inckle, A. E. & Waldron, G. W. J. Aspects of Stage II fatigue crack propagation in low-carbon steel. *J. Mater. Sci.* **6**, 319–323 (1971).

24. Rickerby, D. G. & Fenici, P. Fatigue crack growth in thin section type 316 stainless steel. *Eng. Fract. Mech.* **19**, 585–599 (1984).

25. ASTM E647−13. Standard Test Method for Measurement of Fatigue Crack Growth Rates. *American Society for Testing and Materials* 1–50 (2022) doi:10.1520/E0647-22B.2.

26. Díaz, F. A., Patterson, E. A., Tomlinson, R. A. & Yates, J. R. Measuring stress intensity factors during fatigue crack growth using thermoelasticity. *Fatigue Fract. Eng. Mater. Struct.* **27**, 571–583 (2004).

27. Ziegler, J. F., Ziegler, M. D. & Biersack, J. P. SRIM - The stopping and range of ions in matter (2010). *Nucl. Instruments Methods Phys. Res. Sect. B Beam Interact. with Mater. Atoms* **268**, 1818–1823 (2010).

28. Stoller, R. E. *et al.* On the use of SRIM for computing radiation damage exposure. *Nucl. Instruments Methods Phys. Res. Sect. B Beam Interact. with Mater. Atoms* **310**, 75–80 (2013).

29. Agarwal, S., Lin, Y., Li, C., Stoller, R. E. & Zinkle, S. J. On the use of SRIM for calculating vacancy production: Quick calculation and full-cascade options. *Nucl. Instruments Methods Phys. Res. Sect. B Beam Interact. with Mater. Atoms* **503**, 11–29 (2021).

30. Greene, R. J., Patterson, E. A. & Rowlands, R. E. Thermoelastic Stress Analysis. in *Solid Mechanics and its Applications* vol. 269 743–768 (2008).

31. Díaz, F. A., Yates, J. R. & Patterson, E. A. Some improvements in the analysis of fatigue cracks using thermoelasticity. *Int. J. Fatigue* **26**, 365–376 (2004).

32. Patki, A. S. & Patterson, E. A. Thermoelastic stress analysis of fatigue cracks subject to overloads. *Fatigue Fract. Eng. Mater. Struct.* **33**, 809–821 (2010).

33. Nix, W. D. & Gao, H. Indentation size effects in crystalline materials: A law for strain gradient plasticity. *J. Mech. Phys. Solids* **46**, 411–425 (1998).

34. Yabuuchi, K., Kuribayashi, Y., Nogami, S., Kasada, R. & Hasegawa, A. Evaluation of irradiation hardening of proton irradiated stainless steels by nanoindentation. *J. Nucl. Mater.* **446**, 142–147 (2014).

35. Damcott, D. L., Allen, T. R. & Was, G. S. Dependence of radiation-induced segregation on dose, temperature and alloy composition in austenitic alloys. *J. Nucl. Mater.* **225**,

97–107 (1995).

36. Xia, S., Gao, M. C., Yang, T., Liaw, P. K. & Zhang, Y. Phase stability and microstructures of high entropy alloys ion irradiated to high doses. *J. Nucl. Mater.* **480**, 100–108 (2016).

37. Xu, C. *et al.* Microstructural evolution of reactor internals stainless steel under xenon irradiation studied by GIXRD and positron annihilation technique. *Ann. Nucl. Energy* **96**, 176–180 (2016).

38. Huang, H. F. *et al.* TEM, XRD and nanoindentation characterization of Xenon ion irradiation damage in austenitic stainless steels. *J. Nucl. Mater.* **454**, 168–172 (2014).

39. Huan, D., Li, Y., Chen, X. & Liu, H. Effects of fe11+ ions irradiation on the microstructure and performance of selective laser melted 316l austenitic stainless steels. *Metals (Basel).* **10**, 1–12 (2020).

40. Wang, D., Zhao, L., Xu, L., Han, Y. & Hao, K. A microstructure-based study of irradiation hardening in stainless steel: Experiment and phase field modeling. *J. Nucl. Mater.* **569**, (2022).

41. Jin, H. H., Ko, E., Lim, S., Kwon, J. & Shin, C. Effect of irradiation temperature on microstructural changes in self-ion irradiated austenitic stainless steel. *J. Nucl. Mater.* **493**, 239–245 (2017).

Supplementary Data

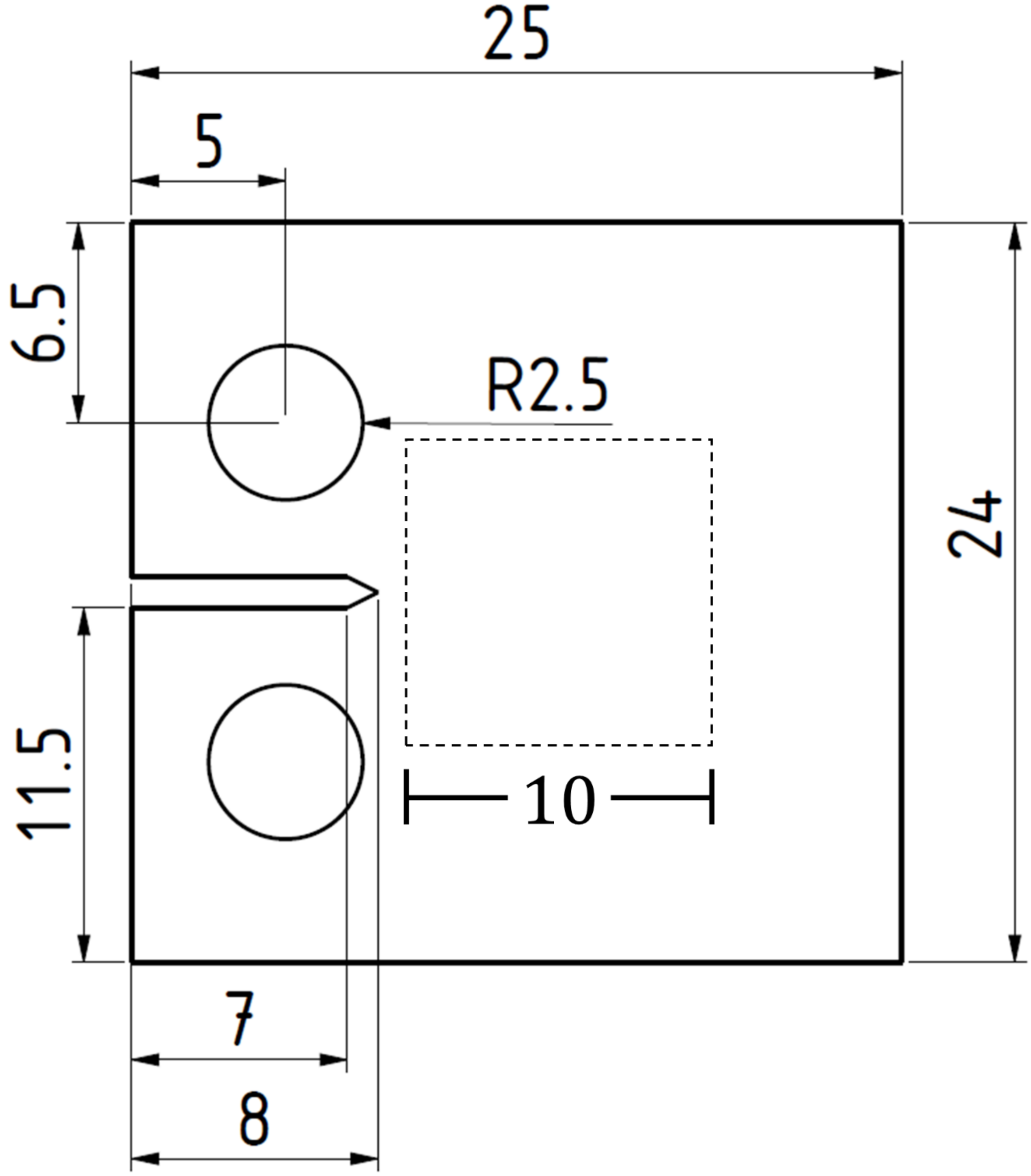

S 1: Dimensions of compact tension specimens used in fatigue tests (dimensions in mm). Specimens were manufactured with a thickness of 1.1 mm, the nominal thickness after polishing reduced to 0.8 mm. The dashed box indicates the irradiated region of the specimen.